Astron. Astrophys. 340, 232–240 (1998)

ASTRONOMY AND ASTROPHYSICS

High–resolution imaging of NH_3 inversion lines toward W3 main

A.R. Tieftrunk[1], **R.A. Gaume**[2], **and T.L. Wilson**[3,4]

[1] ESO/La Silla, Casilla 19001, Santiago 19, Chile
[2] US Naval Observatory, 3450 Massachusetts Avenue NW, Washington, DC 20392-5420, USA
[3] Max Planck Institut für Radioastronomie, Auf dem Hügel 69, D-53121 Bonn, Germany
[4] SMTO, Steward Observatory, The University of Arizona, Tucson, AZ 85721, USA

Received 19 March 1998 / Accepted 27 July 1998

Abstract. Three-arcsecond angular resolution (0.03 pc at 2.3 kpc) images of the (J,K) = (1,1) and (2,2) NH_3 inversion lines toward W3 Main are presented. These observations show NH_3 emission from individual clumps and filaments embedded in the lower density ammonia gas, previously observed with a spatial resolution of 40″. Toward the molecular core W3 East we detect NH_3 emission with broad line profiles from a very compact (FWHM $\approx 5''$) and dense clump toward IRS 5 and weaker emission from compact clumps near IRS 11. The molecular clump toward IRS 5 is associated with a cluster of young low–mass stars and hypercompact H II regions tracing recent high–mass star formation. Toward the molecular core W3 West, which is luminous in the submillimetre but has no embedded H II continuum or NIR sources, we detect NH_3 emission with narrow line profiles from a more extended ($\approx 25''$) and clumpy region. A thin NH_3 filament, less than 8″ wide, stretches more than 40″ away from IRS 4, northeast of W3 West, curving around the compact H II region W3 H. Toward the ultracompact H II region W3 B we find ammonia in absorption. The VLA data presented here are in support of models which suggest that star formation seems to be occurring in bursts toward the W3 GMC. Extended NH_3 emission is detected only toward a quiescent core with no associated star formation. In comparison, toward the active star–forming cores the NH_3 is dispersed and underabundant.

Key words: ISM: abundances – ISM: individual objects: W3 – ISM: molecules – radio lines: ISM

1. Introduction

The W3 giant molecular cloud complex (GMC), situated in the Perseus arm at a distance of $\approx$ 2.3 kpc, hosts two massive and dense star–forming regions, W3 Main in the north and W3(OH) in the south. Far–infrared and submillimetre observations (Werner et al. 1980, Jaffe et al. 1983, Campbell et al. 1989, Ladd et al. 1993) and molecular studies of W3 Main (Wright et al. 1984, Hayashi et al. 1989, Oldham et al. 1994, Tieftrunk et al. 1995, Dickel et al. 1996) further resolve this region into two dense cores, located just south of IRS 4 in the west (W3 West) and toward IRS 5 in the east (W3 East).

High resolution observations have shown that the molecular gas in these cores is densly clustered (Tieftrunk et al. 1995, Roberts et al. 1997). W3 Main has received considerable attention due to its embedded H II regions, which appear to be ionized by a recently formed association of O/B stars (Harris & Wynn-Wiliams 1976, Colley 1980, Roelfsma & Goss 1991, Tieftrunk et al. 1997). The sizes of the H II regions range from 0.01 pc to 1 pc: the more extended of these H II regions are found toward the lower density gas away from the two dense cores; the smallest of the H II regions with diameters of ≤ 2000 AU [hereafter referred to as hypercompact H II regions (Tieftrunk et al. 1997)] are detected toward the infrared sources IRS 4 and IRS 5. Along with IRS 5, a dense cluster of 80 - 240 low–mass stars is embedded in W3 East (Megeath et al. 1996). Intense OH and H_2O maser sources (Wynn-Wiliams et al. 1974, Gaume & Mutel 1987, Claussen et al. 1994) and strong molecular outflows (Bally & Lada 1983, Claussen et al. 1984, Mitchel et al. 1991, Mitchell, Hasegawa & Schella 1992, Choi et al. 1993, Hasegawa et al. 1994) are further evidence of ongoing star formation toward W3 Main.

From their low resolution observations, Tieftrunk et al. 1998 find extended NH_3 emission from the molecular core W3 West, outlined correspondingly by many other molecular tracers. In comparison, however, these low resolution observations do not resolve the molecular core W3 East. In our previous study, we examined the distribution of the ammonia gas in the entire W3 GMC relative to the low density gas, observed stellar clusters and sites of star formation. In this work, we now resolve individual NH_3 emission regions blended at lower resolution and analyze the direct association of the dense ammonia gas with the active star–forming cores toward W3 Main.

2. Observational procedures

The observations were made in April 1995 during a 12 hour observing run using all 27 antennas of the VLA of the NRAO[1] in the D (most compact) configuration. Two analyzing bands, each of width 6.25 MHz, were observed simultaneously and cen-

[1] The National Radio Astronomy Observatory is a facility of the U.S. National Science Foundation operated under cooperative agreement by Assoc. Universities, Inc.

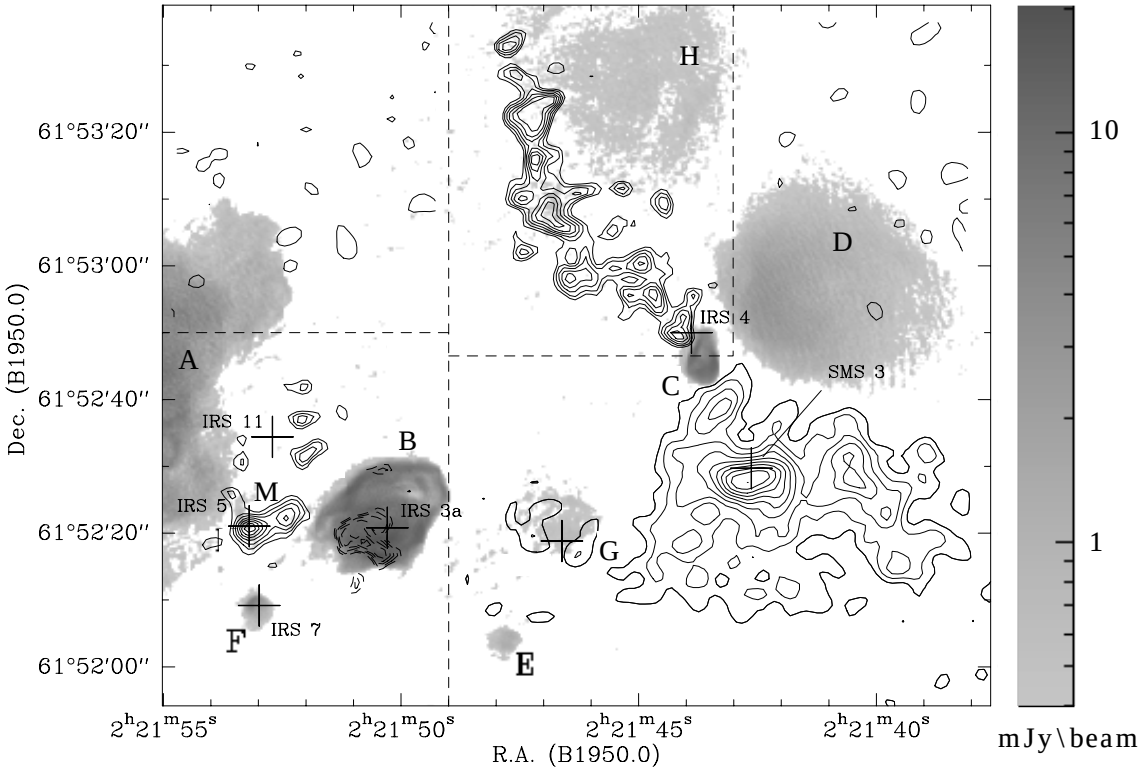

Fig. 1. Overlay of the NH_3(1,1) emission (contours) with the 4.9 GHz continuum emission (grey-scale) from Tieftrunk et al. (1997) toward W3 Main. Letters indicate the H II regions, crosses mark the positions of the NIR sources and SMS 3. The two pointing centers for the NH_3 observations are toward IRS 5 and SMS 3. For comparison, we show the NH_3(1,1) CLEANed natural weighted data from channel -46 km s^{-1} toward the weak filament near W3 H (6 mJy beam^{-1} to 12 mJy beam^{-1} by 1.2 mJy beam^{-1}) and from channel -42.25 km s^{-1} toward SMS 3 (9 mJy beam^{-1} to 45 mJy beam^{-1} by 4.5 mJy beam^{-1}) with the uniform weighted data from channel 38.5 km s^{-1} toward W3 East (6.8 mJy beam^{-1} to 17 mJy beam^{-1} by 1.7 mJy beam^{-1} and dashed contours -5.5 mJy beam^{-1} to -11 mJy beam^{-1} by -1.1 mJy beam^{-1}).

tered on the (J,K) = (1,1) and (2,2) lines, with rest frequencies of 23694.4955 and 23722.6336 MHz. Each band was divided into 63 contiguous channels, each with a frequency width of 97.65625 kHz. The 64th channel is a pseudo continuum channel made up of an average of the inner 75% of the other channels. Channel 32 of each band was centered at -41 km s^{-1}. Since the FWHM primary beam of the individual VLA antennas is approximately 2′ at the 1.3 cm observing wavelength, and since the two regions of interest in W3 Main are over 1′ apart, data were obtained for two different pointing positions: IRS 5, toward the molecular core W3 East at R.A. $2^h21^m53^s$, Dec. 61°52′20″ (B1950.0), and SMS 3, toward the molecular core W3 West at R.A. $2^h21^m43^s$, Dec. 61°52′30″ (B1950.0). [hereafter, all coordinates reported will be given for the B1950.0 epoch]. Approximately four hours of on–source time were allocated for each of the two pointing centers.

The flux density scale was calibrated by observations of 3C 48, which was assumed to have a flux density of 1.1 Jy at 1.3 cm. Phase calibration was accomplished through periodic observations of 0224+671 (2.97 Jy). Bandpass calibration was accomplished through observations of 3C 84. The data were inspected, edited, calibrated, and imaged using the standard AIPS package of NRAO on USNO computer systems. Self–calibration was performed on the higher signal-to-noise continuum channel. The self–calibration gain adjustments were applied to all spectral line channels and no positional adjustments of the self–calibrated maps were necessary. To produce data cubes that contain only line emission (many bright compact H II regions can be found toward W3 Main) a continuum image was constructed from 4 sets of channels devoid of line emission and then subtracted from the data in the UV plane. The UV data were then transformed into 32 image cubes: For the 2 pointing positions and the 2 NH_3 lines, uniform and natural weighted data cubes were produced (2x2x2). Each of these data cubes was produced with and without applying a primary beam correction (x2). Finally cubes of dirty and CLEANed maps were produced to emphasize features at different spatial scales (x2 = 32). Hanning smoothing was applied to the data resulting in a spectral resolution of 2.5 km s^{-1} and a noise equivalent bandwidth of 195.3125 kHz. The spatial resolution of the uniform weighted image cubes is 3.″08 ×2.″63 with a positional angle of -59.9^o. Natural weighting of the UV data provided greater sensitivity at the cost of slightly degraded resolution (4.″32 × 3.″5, p.a. -78.5^o). The natural and uniform weighted data were transformed into images with a pixel size of 0.″8. Final data analysis was done using the GILDAS package of IRAM on HP–UX workstations of SEST.

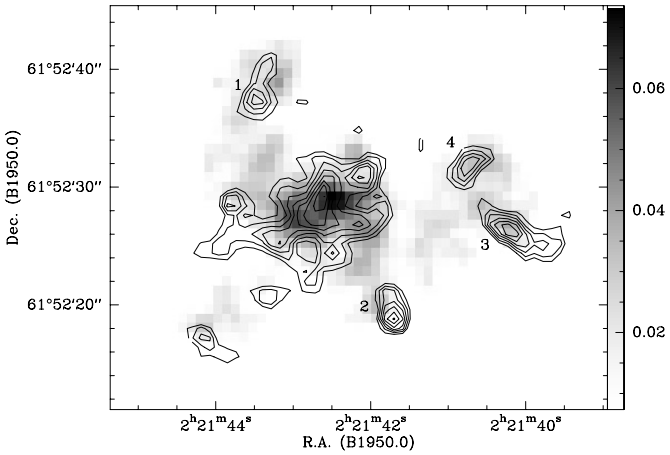

Fig. 2. Channel map of the NH_3(1,1) [contours] and NH_3(2,2) [grey-scale] emission toward W3 West, from the CLEANed and uniform weighted data, integrated over 4 velocity channels from -39.75 $\mathrm{km\,s^{-1}}$ to $-43.5\,\mathrm{km\,s^{-1}}$. Contour levels are from 19.5 $\mathrm{mJy\ beam^{-1}}$ to 65 $\mathrm{mJy\ beam^{-1}}$ by 6.5 $\mathrm{mJy\ beam^{-1}}$; the noise level is 15.8 $\mathrm{mJy\ beam^{-1}}$ r.m.s.

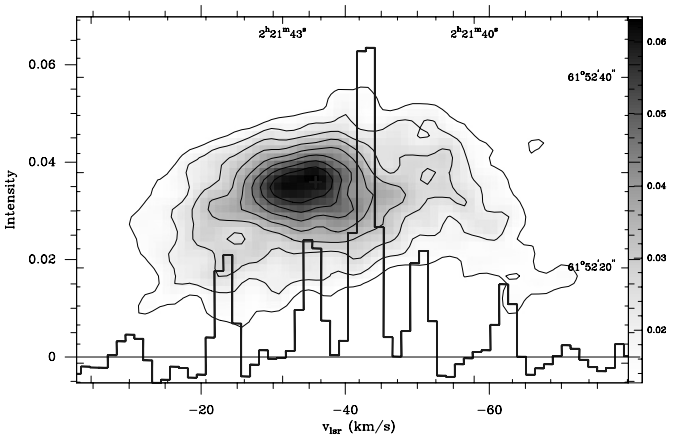

Fig. 3. -43.5 $\mathrm{km\,s^{-1}}$ channel map from the dirty and natural weighted NH_3(1,1) data obtained toward SMS 3. Superimposed is the NH_3(1,1) spectrum obtained toward the core center, which is coincident with the position of SMS 3. Contour levels are 12.8 $\mathrm{mJy\ beam^{-1}}$ to 64 $\mathrm{mJy\ beam^{-1}}$ by 6.4 $\mathrm{mJy\ beam^{-1}}$. The noise level is 7.9 $\mathrm{mJy\ beam^{-1}}$ r.m.s.

3. Results

In Fig. 1 we show the NH_3(1,1) emission toward W3 Main from the CLEANed natural weighted data obtained toward the pointing center SMS 3 and the uniform weighted data obtained toward IRS 5. We use the differently weighted data sets to show *all* of the detected features in spatial relation with each other, including compact with extended and weak with strong NH_3 emission. Thus, the contour levels are different for the insets at bottom left and top center (see caption) to enhance the weak features in relation to the strong NH_3(1,1) main emission toward W3 West. We include a grey-scale image of the 4.9 GHz continuum emission, observed toward W3 Main at $0\farcs46$ resolution by Tieftrunk et al. (1997), to identify the H II and IR sources we will refer to throughout this paper. A logarithmic scale has been used and intensified at the low end to display the weak emission features (for true fluxes see Tieftrunk et al. 1997). Crosses identify the positions of the strong submillimetre source SMS 3 (Ladd et al. 1993) and the near–infrared sources. The H II regions are labeled according to Wynn-Wiliams (1971) and Harris & Wynn-Wiliams (1976).

Due to its greater sensitivity, the natural weighted data are best suited to detect extended low brightness emission, as toward W3 West shown in Fig. 1. However, due to its lower resolution, it is not tailored to resolve compact objects embedded in such emission regions. This is demonstrated in Fig. 2, where we show the NH_3(1,1) and (2,2) emission toward W3 West, taken from the CLEANed and uniform weighted data. From Fig. 1 it is already apparent that the NH_3 emission toward W3 West is clumpy. Using spatially coincident NH_3(1,1) and (2,2) emission from the uniform weighted data as selection criteria, we resolve at least 4 compact NH_3 clumps with diameters of FWHP $\approx 4''$, surrounding the core emission of W3 West toward SMS 3.

Since the CLEAN deconvolution algorithm occasionally performs poorly in regions of weak, extended emission, we also analyzed the dirty data cubes for each pointing. Fig. 3 shows the -43.5 $\mathrm{km\,s^{-1}}$ channel map of the NH_3(1,1) emission toward W3 West and the NH_3(1,1) spectrum toward its core at the position of SMS 3, obtained from the dirty and natural weighted data. The clumpiness of this molecular core is now no longer apparent. NH_3(1,1) emission is detected in a region of FWHP $\approx 25''$; traced in $C^{18}O$ the W3 West core has a size of FWHP $\approx 40''$ (Tieftrunk et al. 1995).

Fig. 4 shows the dirty and natural weighted NH_3(1,1) data obtained toward W3 East and integrated over 5 channels from -37.25 $\mathrm{km\,s^{-1}}$ to -42.25 $\mathrm{km\,s^{-1}}$. Thus, all of the weak NH_3(1,1) emission detected with the VLA toward W3 East is shown in this image. As opposed to W3 West, no extended low brightness NH_3(1,1) emission can be detected tracing the molecular core W3 East, which has a diameter of FWHP $\approx 25''$ when traced in $C^{18}O$ (e.g. Tieftrunk et al. 1998). The central ammonia clump is located at R.A. $2^{\mathrm{h}}21^{\mathrm{m}}53.2^{\mathrm{s}}$, Dec. $61^{\circ}52'21''$. Thus, it is centered on IRS 5 and the hypercompact H II cluster W3 M (Tieftrunk et al. 1997). From the CLEANed and natural weighted NH_3(1,1) and (2,2) data obtained at a resolution of $3''$ toward IRS 5, we find this clump to be highly centrally condensed and possibly spatially unresolved.

Fig. 5 shows a closeup of the $-38.5\,\mathrm{km\,s^{-1}}$ NH_3(1,1) channel map of the CLEANed and uniform weighted data obtained toward IRS 5. NH_3 in absorption is detected toward the south-eastern edge of W3 B, where the cm–continuum emission is brightest and the H66α recombination line emission shows the broadest linewidths (Roelfsma & Goss 1991, Tieftrunk et al. 1997). The compact source IRS 3a, most likely the exciting source of W3 B (Megeath et al. 1996), is $\approx 4''$ to the west and $\approx 2''$ to the north of this position. The spectrum shown has been taken at R.A. $2^{\mathrm{h}}21^{\mathrm{m}}51.2^{\mathrm{s}}$, Dec. $61^{\circ}52'19\farcs5$. Also visible in this image is the ammonia clump toward W3 M/IRS 5 and a string

Table 1. NH_3(1,1) and (2,2) line parameters toward W3

Region	R.A. [$2^h21^m\downarrow^s$]	Dec. [$61°52'\downarrow''$]	T_{MB}(1,1) [K]	$\Delta v_{1/2}{}^\star$ [km s^{-1}]	T_{MB}(2,2) [K]	$\Delta v_{1/2}{}^\star$ [km s^{-1}]	v_{lsr} [km s^{-1}]
W3 West*	42.6	29.0	13.0±1.5	3.2±0.3	9.2±1.0	< 2.5	-42.8±0.2
IRS 4*	44.5	50.5	3.1±0.4	4.5±0.6	2.8±0.3	3.0±0.5	-47.1±0.2
clumps •	toward SMS 3		3.8±0.7	< 2.5	4.0±0.7	< 2.5	$\approx -42 \pm 1$
IRS 5*	53.2	21.0	4.1±0.5	5.7±0.7	6.5±0.7	5.6±0.7	-38.2±0.2
clumps •	toward IRS 11		2.3±0.3	< 2.5	2.7±0.3	< 2.5	$\approx -39 \pm 1$
W3 B •	51.2	19.5	-2.3±0.3	3.2±0.3	-1.8±0.2	< 2.5	-38.3±0.3

* NATURAL WEIGHTED;
• UNIFORM WEIGHTED;
⋆ LINEWIDTHS ARE *not* DECONVOLVED FROM 2.5 km s^{-1} INSTRUMENTAL RESOLUTION.

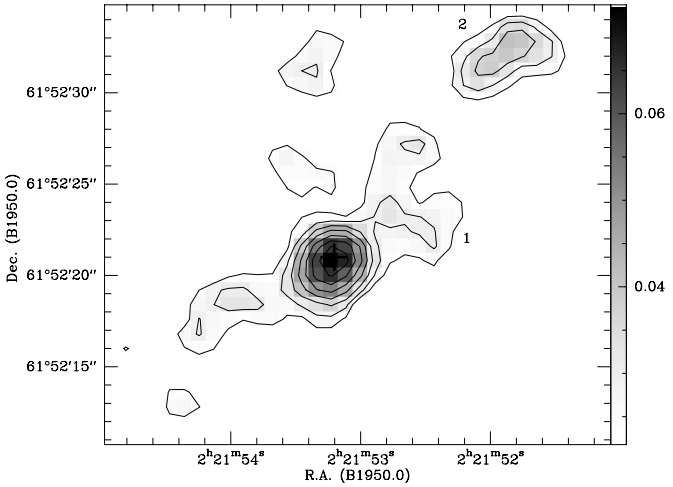

Fig. 4. Contour plot of the NH_3(1,1) emission toward IRS 5, from the dirty and natural weighted data, integrated over 5 velocity channels from -37.25 km s^{-1} to -42.25 km s^{-1}. Contour levels are from 21.6 mJy beam^{-1} to 72 mJy beam^{-1} by 7.2 mJy beam^{-1}. The noise level is 17.7 mJy beam^{-1} r.m.s.

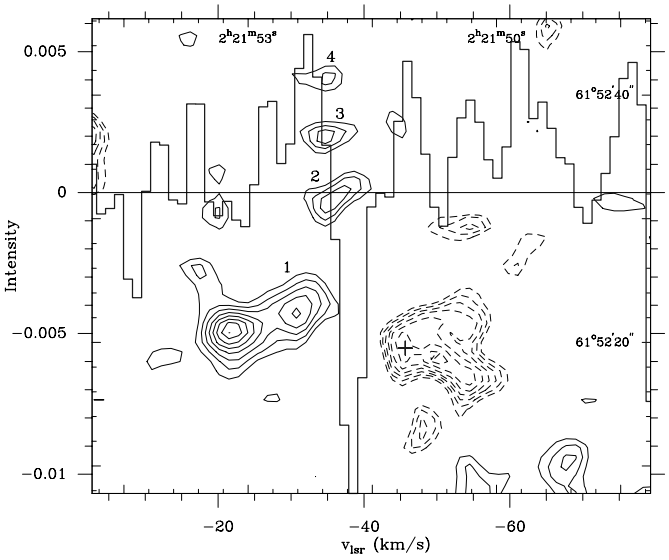

Fig. 5. -38.5 km s^{-1} channel map from the CLEANed and uniform weighted NH_3(1,1) data obtained toward IRS 5. Contour levels are 6.4 mJy beam^{-1} to 16.6 mJy beam^{-1} by 1.7 mJy beam^{-1} for the emission; dashed contour levels are -11 mJy beam^{-1} to -5 mJy beam^{-1} by 1 mJy beam^{-1} for the absorption. The weaker emission peaks are numbered. Superimposed is the NH_3(1,1) spectrum obtained toward the position of maximum absorption, indicated by the cross. The noise level is 7.9 mJy beam^{-1} r.m.s.

of less brighter clumps northwest of it. The clumps are $\approx 3''$ west of IRS 11, which has a similar north–south elongation (cf. K–band image in Fig. 2 of Hayward et al. 1989) aligned with the string of clumps. IRS 11 is associated with a dense CO clump (Tieftrunk et al. 1995), showing a warm dust component (Hayward et al. 1989), but no H II continuum emission (cf. Fig. 9 in Tieftrunk et al. 1997).

Fig. 6 shows the NH_3(1,1) and (2,2) spectra obtained from the CLEANed and natural weighted data toward SMS 3, i.e. the center of W3 West, and IRS 5 in W3 East. The CLEANed and natural weighted data are best suited to obtain reliable intensities for comparison and accurate intensity ratios for the HF components of the NH_3 inversion lines. The spectra shown contain only line emission. The continuum emission constructed from 4 sets of channels devoid of line emission was subtracted from these data in the UV plane and no additional baselines were removed. The line parameters obtained by fitting NH_3 line profiles (i.e. assuming a fixed velocity distribution, equal linewidths and equal excitation temperatures for the main and HF components) are given in Table 1, along with the errors derived by this NH_3 fit–method. Toward SMS 3 the NH_3 line profiles are narrow when compared to IRS 5. The NH_3(1,1) and (2,2) linewidths toward IRS 5 are the largest measured in our data. Here, the NH_3(1,1) main component is blended with the first HF components. Also, the NH_3(2,2) line is broadened in comparison to the NH_3(2,2) line profile from SMS 3. For the NH_3(1,1) emission we find optical depths τ of $1 - 1.5$ and $2 - 3$ for IRS 5 and SMS 3, respectively. This is considerably larger than the apparent optical depths obtained from the single–dish data by Tieftrunk et al. (1998). Optical depths for the NH_3(2,2) emission are small.

A comparison between the VLA and 100-m NH_3 line intensities shows that the molecular gas toward W3 Main is indeed highly clumped. From the 100-m data, Tieftrunk et al. (1998) found optically thin line emission toward the core of W3 West. Toward the position of IRS 5 they found only weak line broad-

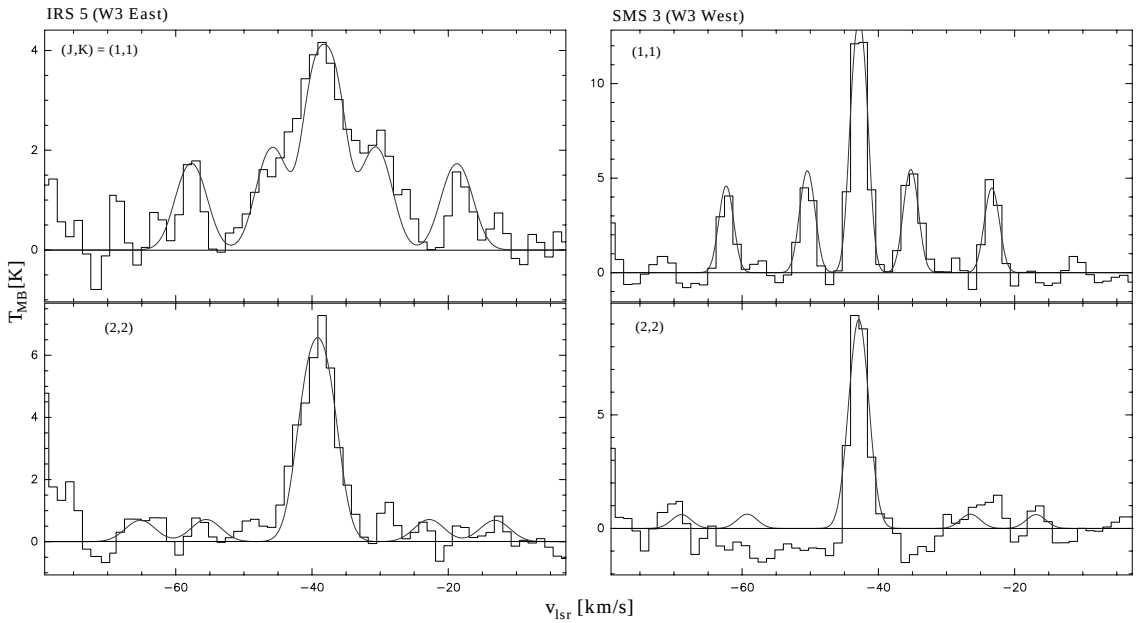

Fig. 6. NH_3(1,1) and (2,2) spectra toward IRS 5 in W3 East (left) and SMS 3 in W3 West (right) obtained from the CLEANed and natural weighted data.

ening and peak intensities $\approx$ 4 times weaker when mapped at 40″ resolution. Toward W3 B the NH_3(1,1) and (2,2) lines were detected in emission, not absorption. The filamentary emission northeast of IRS 4 was not resolved, but blended with the NH_3 emission from W3 West in the 40″ beam. Thus, it is clear that the line emission mapped with the 100-m must have been strongly affected by beam dilution, given the very compact embedded clumps we detect with the VLA at high resolution. Comparing the total flux and size of the NH_3(1,1) emission region detected with the VLA toward W3 West with that detected with the 100-m, the VLA records less than 60% of the weaker emission mapped with the single–dish.

In Table 1 we also give the line parameters we find from the primary beam corrected CLEANed and uniform weighted data for the very compact ammonia clumps toward SMS 3 (cf. Fig. 2) and the absorption region and clumps near IRS 11 (cf. Fig. 5). For these clumps we find the optical depths to be around unity. Note, that the reported linewidths are convolved with our instrumental resolution of 2.5 $\mathrm{km\,s^{-1}}$ after Hanning smoothing the data to obtain a higher signal-to-noise ratio. Since the NH_3(1,1) and (2,2) emission peaks from the ammonia clumps toward W3 West and near IRS 11 are one or two channels broad, their linewidths are unresolved at our spectral resolution.

The NH_3 line parameters have been used, following the methods outlined in the Appendix of Wilson et al. (1993), to deduce the cloud parameters given in Table 2. The errors have been derived subsequently from the uncertainties in the NH_3 line profile fits to our data. Since only the NH_3(1,1) and (2,2) inversion lines have been measured, our data are most sensitive to gas cooler than 100 K. The NH_3 data provide estimates for T_{kin} (e.g. Danby et al. 1988), virial masses (from FWHP linewidths and clump radii assuming virial equilibrium), NH_3 column densities (assuming an LTE population, characterized by a single T_{rot} for the metastable levels), H_2 densities (from source size and virial mass), and relative abundance of NH_3 to H_2 (from virial masses, assuming a uniform density and spherical geometry). Note that the virial masses for the dense ammonia clumps are upper limits if the linewidths and clump sizes are unresolved at our resolutions of 2.5 $\mathrm{km\,s^{-1}}$ and $\approx$ 0.03 pc, respectively. The parameters we found for the small clumps toward SMS 3 and near IRS 11 are also given in Table 2. They are comparable to those values found from VLA measurements for the dense and compact ammonia clumps detected toward W3(OH) by Wilson et al. (1993) or DR 21 by Wilson et al. (1995). T_{rot}, $N(NH_3)$, $n(H_2)$ and τ determined toward IRS 5 and SMS 3 are in excellent agreement compared to values of optical depths as a function of densities and temperatures when derived from detailed NH_3 excitation models as presented by Kuiper (1994).

4. Discussion

Luminous IR sources detected toward W3 Main have mostly been associated with compact or ultracompact H II regions surrounding them (e.g. Roelfsema & Goss 1991). Of these, only a few appear to be still embedded in dense molecular gas (Tieftrunk et al. 1997). An anti–correlation between the *expanded* H II regions and the molecular gas toward W3 Main had been noted previously for H_2 densities of $10^4 - 10^5$ $\mathrm{cm^{-3}}$ (Tieftrunk et al. 1995, 1998, Roberts et al. 1997). In W3 Main, Tieftrunk et al. (1998) found strong and extended NH_3 emission only toward the quiescent molecular cores W3 West and W3 SE (not included in the VLA maps presented here), which have no embedded NIR sources or ultracompact H II regions. They found the relative NH_3 abundance within the dense molec-

Table 2. NH_3 cloud parameters

Region	r [10^{-2}pc]	M_{vir} [$M_\odot$]	T_{rot} [K]	T_{kin} [K]	$N(NH_3)$ [$10^{14}cm^{-2}$]	$n(H_2)$ [$10^6 cm^{-3}$]	$X(NH_3)$ [10^{-9}]
W3 West	14	$300-400$	25±5	35±10	27±5	$0.5-0.7$	$4-7$
IRS 4*	2	$50-130$	30±5	45±10	8±2	$30-80$	$0.1-0.3$
IRS 5*	3	$60-240$	50±10	180±100	15±5	$10-40$	$0.1-1.0$
clumps•	2	<30	35±10	55±30	6±2	$10-30$	$0.1-0.6$
W3 B	3	$60-90$	25±5	35±10	5±2	$10-16$	$0.1-0.4$

* VALUES ARE DERIVED FOR NARROW AND BROAD LINEWIDTHS, CF. SECT. 4.1. & 4.2.;
• VIRIAL MASSES ARE UPPER LIMITS IF LINEWIDTHS AND CLUMP SIZES ARE UNRESOLVED.

ular clumps actively forming stars to be lower and that, once embedded young stellar objects emerge from these clumps to become visible as ultracompact H II regions, the NH_3 is quickly dispersed.

4.1. W3 West

From our high resolution observations, we detect extended NH_3(1,1) and (2,2) emission only toward the W3 West molecular core. For this core, we find a FWHP diameter ≈ 60% of that found by mapping the core with other dense molecular gas tracers at lower resolution. From the $C^{18}O$ data of Tieftrunk et al. (1995) and the ^{13}CO data of Roberts et al. (1997), it has been shown that molecular clumps with masses of ≈ 100 $M_\odot$ are embedded in the molecular gas toward W3 West. The NH_3 emission must not necessarily trace the same intensity peaks found from $C^{18}O$ and ^{13}CO emission, but we detect NH_3 emission peaks from several compact dense clumps, for which we derive virial masses of ≈ 30 $M_\odot$ with H_2 densities of order 10^7 cm^{-3}. The W3 West core, from our NH_3 data, has a virial mass of $300-400$ $M_\odot$. From this, the average density of $n(H_2)$ is $5-7\times10^5$ cm^{-3}, which compares well to the average density of 7×10^5 cm^{-3} derived from $C^{34}S$ LVG analysis of the core emission (Tieftrunk et al. 1998).

Although compact NIR emission and H II sources have been detected only toward the perimeter of the W3 West molecular core, a compilation of infrared and submillimetre observations by Ladd et al. (1993) shows that the center of this core, SMS 3, is very luminous in the submillimetre. The SMS 3 core, when traced in 450 and 800 μm emission, envelopes the compact clumps we find toward the center of W3 West. SMS 3, however, has not been detected at wavelengths shorter than 100 μm. This indicates a lack of hot dust and suggests that, if star formation is associated with the dense ammonia clumps in the W3 West molecular core (as toward IRS 5/SMS 1 and IRS 4/SMS 2), any embedded source may still be too enshrouded to be visible in the NIR. From our data we find average NH_3 column densities of a few times 10^{15} cm^{-2} for the W3 West core and derive a relative NH_3 abundance of $4-7\times10^{-9}$, in good agreement with $X(NH_3)$ derived by Tieftrunk et al. (1998).

Ammonia emission from a compact and dense clump is also detected toward W3 Ca/IRS 4. Note that this clump is not toward the ultracompact H II region W3 C, but rather northeast of it, toward the hypercompact H II region W3 Ca, which has been associated with IRS 4 (Tieftrunk et al. 1997). The clump is part of a filamentary structure traced in NH_3, which stretches away more than 40″ to the northeast, tracing the outer edge of the extended diffuse H II region W3 H. This filament is very clumpy along its profile. The linewidths from the NH_3(1,1) and (2,2) emission toward the filament are < 2.5 $km\ s^{-1}$, thus this gas appears to be more quiescent than the NH_3 gas near IRS 4, where the emission is stronger and the second broadest NH_3 linewidths in our data were found (cf. Table 1).

A possible outflow associated with IRS 4 has been discussed by Hasegawa et al. (1994) and may have a significant effect on the molecular line broadening. However, from the v_{lsr} gradients detected north of IRS 4, it is more likely that the champagne flow of the expanding W3 C region (Roelfsma & Goss 1991) is affecting the molecular gas. From position–velocity analysis of our NH_3 data, we find the northern part of the filament to be at more positive velocities compared to the southern end, in accordance with the velocity gradient found for the champagne flow of the ionized gas. Thus, the molecular line broadening of the NH_3 emission toward W3 C may be caused by an interaction with this expanding gas itself (Hasegawa et al. 1994). For comparison, we derive the clump parameters in Table 2 using the presumably unbroadened linewidths from the lower resolution NH_3 data of Tieftrunk et al. (1998) and the linewidths measured in our high resolution data to estimate a virial mass of $50-130$ $M_\odot$ and a total density of $n(H_2) = 3-8\times10^7$ cm^{-3}. We derive a relative NH_3 abundance of a few times 10^{-10}, an order of magnitude lower than toward SMS 3.

4.2. W3 East

Ammonia emission was detected toward the W3 East molecular core from 100-m observations by Tieftrunk et al. (1998). From our VLA data we find this emission to arise from a very compact NH_3 clump toward IRS 5. Ammonia is not detected throughout the molecular core W3 East itself, although extended emission from dense molecular gas between W3 A and W3 B is traced toward this core (cf. Fig. 8 in Tieftrunk et al. 1998). IRS 5 is associated with the cm–continuum emission from a group of hypercompact objects (cf. Fig. 7 in Tieftrunk et al. 1997). These sources are known to be deeply embedded in a dense molecular clump ($n(H_2) = 3\times10^6$ cm^{-3}) traced in ^{13}CO, $C^{18}O$ and

$C^{34}S$ (Tieftrunk et al. 1995, Roberts et al. 1997) with a virial mass of ≈ 100 $M_\odot$. IRS 5 is also associated with an extremely powerful molecular outflow (Choi et al. 1993, Hasegawa et al. 1994). An interaction of the NH_3 gas with this outflow may explain the broad NH_3 emission line profiles detected in our data toward the IRS 5 clump (cf. Fig. 6). For comparison, we derive the clump parameters in Table 2 using the linewidths from the lower resolution NH_3 data of Tieftrunk et al. (1998) and those measured in our high resolution data. Thus, we estimate a virial mass of $60-240$ $M_\odot$ and a total density of $n(H_2) = 1-4\times10^7$ cm^{-3} for this clump. We derive a relative NH_3 abundance of $1-10\times10^{-10}$, an order of magnitude lower than toward SMS 3 in W3 West. This is in good agreement with $X(NH_3)$ derived by Tieftrunk et al. (1998), who proposed that the winds and radiation from the embedded stars and the expanding hypercompact H II regions must have a significant impact on the NH_3 and its chemistry in this highly active star–forming core, lowering the relative NH_3 abundance without dispersing the dense molecular core itself yet. Depletion of NH_3 inside this active core is unlikely; from chemical evolution models of protostellar cores, Bergin & Langer (1997) found that for high densities ($> 10^6$ cm^{-3}) NH_3 does not necessarily deplete onto grains, even at low temperatures (T_{gas}= T_{dust} = 10 K). Low $X(NH_3)$ has also been detected for the H_2O maser clump toward W3(OH) (Wilson et al. 1993), which is associated with the Turner–Welch (TW) object, a luminous millimetre–continuum source considered to be the high–mass equivalent of a class 0 object (Turner & Welch 1984, Wilner et al. 1995). For other examples of low $X(NH_3)$-values toward high–mass star–forming cores with embedded IR sources, see also the discussion of Davis & Dent (1993).

IRS 11, which has also been shown to be embedded in a dense $C^{18}O$ clump (Tieftrunk et al. 1995), shows no cm–continuum emission (cf. Fig. 1), but based on their photometric analysis Hayward et al. (1989) deduce that the near-IR emission must arise from young stellar objects deeply embedded in molecular gas. The direct spatial association of IRS 11 with the compact ammonia clumps 3″ west of it is not assured, but the K–band images of Hayward et al. (1989) show a striking similarity in the morphology of IRS 11 to the north–south alignment of these ammonia clumps. In fact, the K–band mosaic of Megeath et al. (1996), obtained at higher resolution, resolves IRS 11 into three, possibly four individual sources (cf. Fig. 1a in Megeath et al. 1996). The southernmost of these sources appears to be the brightest, with a small nebulosity extending north, but detailed photometry of the individual NIR sources at the higher resolution has not been carried out. Megeath et al. (1996) also find a small stellar cluster toward IRS 5, $\approx 7''$ west of IRS 11. Alignment of our data with their K–band image shows the ammonia clumps to fall between IRS 11 and the cluster, so an association of the ammonia clumps with the corresponding NIR sources remains somewhat elusive. Their vicinity to IRS 5 itself may also link them to the powerful outflow emanating from IRS 5 (Choi et al. 1993, Hasegawa et al. 1994). For the ammonia clumps we estimate virial masses of ≈ 30 $M_\odot$ with H_2 densities of order 10^7 cm^{-3} and $X(NH_3)$ $1-6\times10^{-10}$. Thus, they are comparable to those clumps embedded in the W3 West molecular core.

Toward W3 B, Tieftrunk et al. (1995) found a minimum in the $C^{18}O$ and $C^{34}S$ emission. We find ammonia in absorption coming from a small region within less than 5″ of IRS 3a toward the edge of W3 B. Since we do not detect NH_3 in emission away from the H II region ionized by IRS 3a, we assume that the ammonia is spread out in a thin gaseous layer in front of W3 B, rather than contained in a molecular clump. For comparison with the other emission regions, however, we derive cloud parameters in Table 2 adopting a uniform morphology. Thus, the virial mass of $60-90$ $M_\odot$ we find, with $n(H_2)$ of 10^7 cm^{-3} and $X(NH_3)$ a few times 10^{-10}, should be considered upper limits.

4.3. NH_3 *as tracer of sequential star formation*

At 3″ angular resolution we find no NH_3 emission toward any of the (ultra-)compact H II regions in W3 Main, except for W3 B, where we find NH_3 only in absorption. The lack of NH_3 toward (ultra-)compact H II regions does not necessarily imply the lack of dense molecular gas toward them. From comparison of $C^{18}O$ and H II continuum observations, for example, we know that the cometary ultracompact H II region W3 F, south of IRS 5, is forming its bow–shocked bright rim toward dense gas in W3 East (Tieftrunk et al. 1997). However, we find no NH_3 emission toward this region. Tieftrunk et al. (1998) suggested that toward the very dense IRS 5 molecular clump, where we confirm the relative NH_3 abundance to be low, the ammonia gas is underabundant in the otherwise dense gas because it has preferentially been disrupted by the energetic processes associated with the star formation toward IRS 5. From our observations, we can only infer that gaseous ammonia must be rapidly destroyed by the physical energies prevalent near expanding H II regions correlated with recent high–mass star formation, e.g. an increased UV flux, powerful outflows, massive winds, and expanding shock fronts associated with the young stellar sources.

Considering the various morphologies of the NH_3 emission regions near star-forming cores when mapped at high resolution (e.g. extended cores, compact clumps, thin filaments), ammonia appears to be a good tracer of the signatures of the fundamental processes of *intermediate scale triggered star formation* as discussed in detail by Elmegreen (1998) in the *collect and collapse* scenario. If we were to derive an evolutionary sequence from this scenario for the W3 Main molecular cloud based on our NH_3 observations, we would have to begin with the extended core W3 West. Observing W3 Main in ammonia at lower resolution, W3 West would appear to be associated with the (ultra-)compact H II sources W3 A, B, C or D. However, at higher resolution it becomes evident that no high–mass star formation traced by ultracompact H II regions is detected toward this molecular core. W3 West may be a quiescent molecular core not forming any high–mass stars. Yet, the detection of embedded compact and dense ammonia clumps in the luminous

submillimetre core seems to indicate, that star formation may be occurring deep inside of this molecular core.

If such dense and compact ammonia clumps are associated with early signs of high–mass star formation, then the clumps toward IRS 11, which has no cm–continuum emission, and IRS 4 and 5, where only hypercompact cm–continuum sources were detected at sub–arcsecond resolution (Tieftrunk et al. 1997), may be indicative of very recent high–mass star formation. Once the stellar sources emerge from their dense natal clumps, they appear to destroy the ammonia gas inside these clumps (among other fragile molecules) as suggested by the data of Tieftrunk et al. (1998) and our VLA data. Eventually, ultracompact H II regions will form and expand, ionizing and dispersing the molecular gas around them. This has probably occured toward IRS 3a, where the NH_3 appears to have been swept up into a thin sheet of gas in front of the ionization and shock front and is now detected only in absorption toward the southeastern edge of the expanding ultracompact H II region W3 B.

If molecular gas is being swept up by an expanding H II region before entirely disrupting it, then the ammonia filament along the eastern perimeter of W3 H may be such a swept–up layer. The filament appears to contain several ammonia clumps, the densest one in the south toward IRS 4. If such filaments are further heated and compressed by expanding H II regions, as suggested by Wilson et al. (1993), they may collapse along pre–existing dense condensations. Such condensations appear to exist along this filament, with the clump toward IRS 4 apparently forming new high–mass stars as indicated by the embedded hypercompact H II region W3 Ca (Tieftrunk et al. 1997). As only the densest molecular clumps would collapse along such a filament before it is dispersed, the isolated compact and dense ammonia clumps between W3 A and W3 B, near IRS 11 and toward IRS 5, where high–mass star formation seems to have occured most recently, could also be the remnants of such a collapsed filament as their north–south alignment seems to suggest. One could speculate that the high-mass stars ionizing W3 A (IRS 2,2a,2b,2c) and W3 B (IRS 3a) must also once have been embedded in dense molecular gas, which can now no longer be detected toward either of the compact H II regions. If this gas has been swept up, heated and compressed by the expanding H II regions (Wilson et al. 1993), IRS 5 and IRS 11 may well be sites of subsequent or sequentially triggered star formation.

Since W3 Main has such an abundance of H II regions in different evolutionary phases, the molecular gas is also destined to show a very complex morphology. In order to corroborate the ability of NH_3 to trace the different stages of molecular cloud evolution during its star–forming cycles in such a detailed way as suggested here, more high resolution NH_3 maps of other complex star–forming regions are needed.

5. Conclusions

High sensitivity 3″ angular resolution maps in the (J,K) = (1,1) and (2,2) inversion lines of NH_3, from two separate pointings toward W3 West and W3 East, have given a detailed picture of the distribution of the ammonia gas and its association with high–mass star formation toward W3 Main. From these data, we detect ammonia in extremely compact and highly condensed clumps toward infrared sources which, based on their associated hypercompact H II regions, may host extremely young stellar objects. These clumps exhibit total densities, $n(H_2)$, of a few times 10^7 cm^{-3}, relative NH_3 abundances, $X(NH_3)$, of order 10^{-10} and kinetic temperatures of $\approx 50-250$ K. We reason that NH_3 must be rapidly disrupted *inside* the dense star–forming molecular clumps and dispersed in the molecular gas surrounding them, once stars emerge from their natal cores and the (ultra-)compact H II regions begin to expand around them. We find that lower density ammonia gas can be swept up in filaments, tracing the boundary of these expanded H II regions.

For the more extended ammonia gas in the quiescent W3 West core, which has no associated IR sources but exhibits strong submillimetre emission, we find cooler (35 K) gas with average densities $n(H_2) \approx 6 \times 10^5$ cm^{-3} and $X(NH_3) = 4 - 7 \times 10^{-9}$. The widespread ammonia toward W3 West may be an indication for a still early stage of this molecular core's evolutionary process in forming stars. Although this source would *appear* to be associated with (ultra-)compact H II regions when observed at lower resolution, the high resolution images show that the NH_3 is *not* correlated with this H II continuum emission. Our VLA images show that dense ammonia clumps are embedded in the molecular core W3 West. The densities and relative NH_3 abundancies of these clumps are comparable to those which show associated star formation toward IRS 4, IRS 5 or IRS 11. Considering the luminous submillimetre emission associated with the core of W3 West, these clumps then may be precursors for star formation or indicate that star formation is occurring deeply inside of W3 West, the embedded sources still too enshrouded to be visible in the NIR.

In conclusion, although dense ammonia gas appears to be a good tracer for regions of active star formation, it becomes apparent that at better than 0.1 pc linear resolution, the morphology of the molecular gas traced in NH_3 becomes quite complex. Lower density and spatially extended NH_3 emission detected near (ultra-) compact H II regions apparently traces more quiescent gas not necessarily associated with the active high–mass star formation itself. Dense ammonia clumps embedded in these regions, however, may be signs of prospective star formation. The impression that, relative to the NH_3 abundance in the surrounding gas, a lower X-value for NH_3 in dense clumps is *correlated* with active star formation embedded in these clumps needs to be corroborated. Our observations suggest, however, that the NH_3 abundance and disposition in high–mass star–forming regions changes quickly with the onset of star formation. Considering the transition time from hypercompact H II regions, we correlate with dense compact ammonia cores, to ultracompact H II regions lacking NH_3 emission, the ammonia gas appears to be disrupted within $10^3 - 10^5$ years after the initial formation of an expanding ionized shell around the young high–mass stars.

Thus, very dense, hot and compact ammonia clumps appear to be good tracers of the early stages of high–mass star formation, whereas other dense molecular gas tracers, like $C^{18}O$ or $C^{34}S$, do not seem to allow for such a distinction as they do not adapt as quickly to their changing stellar environment. Our observations merit further high resolution studies of the association of NH_3 with active star–forming regions and more detailed analysis of its role in the chemistry involved.

References

Bally J., Lada C. J., 1983, ApJ 265, 824
Bergin E. A., Langer W. D., 1997, ApJ 486, 316
Campbell M. F., Lester D. F., Harvey P. M., Joy M., 1989, ApJ 345, 298
Choi M., Evans N. J., Jaffe D. T., 1993, ApJ 417, 624
Claussen M. J., Berge G. L., Heiligman G. M., et al., 1984, ApJ 285, L79
Claussen M. J., Gaume R. A., Johnston K. J., Wilson T. L., 1994, ApJ 424, L41
Colley D., 1980, MNRAS 193, 495
Danby G., Flower D. R., Valiron P., Schilke P., Walmsley C., 1988, MNRAS 235, 229
Davis C. J., Dent W. R. F., 1993, MNRAS 261, 371
Dickel H. R., Goss W. M., Condon G., 1996, ApJ 460, 716
Elmegreen B. G., 1998, in Woodward C. E., Thronson H. A., Shull M. (eds.), Origins of Galaxies, Stars, Planets and Life. ASP Conf. Ser.
Gaume R. A., Mutel R. L., 1987, ApJS 65, 193
Harris S., Wynn-Williams C. G., 1976, MNRAS 174, 649
Hasegawa T. I., Mitchell G. F., Matthews H. E., Tacconi L., 1994, ApJ 426, 215
Hayashi M., Kobayashi H., Hasegawa T., 1989, ApJ 340, 298
Hayward T. L., Grasdalen G. L., Woodward C. E., et al., 1989, ApJ 345, 894
Jaffe D. T., Hildebrand R. H., Keene J., Whitcomb S. E., 1983, ApJ 273, L89
Kuiper T. B. H., 1994, ApJ 433, 712
Ladd E. F., Deane J. R., Sanders D. B., Wynn-Williams C. G., 1993, ApJ 419, 186
Megeath S. T., Herter T., Beichmann C., et al., 1996, A&A 307, 775
Mitchell G. F., Hasegawa T. I., Schella J., 1992, ApJ 386, 604
Mitchell G. F., Maillard J.-P., Hasegawa T. I., 1991, ApJ 341, 371
Oldham P. G., Griffin M. J., Richardson K. J., Sandell G., 1994, A&A 284, 559
Roberts D. A., Crutcher R. M., Troland T. H., 1997, ApJ 479, 318
Roelfsema P. R., Goss W. M., 1991, A&AS 87, 177
Tieftrunk A. R., Gaume R. A., Claussen M. J., Wilson T. L., Johnston K. J., 1997, A&A 318, 931
Tieftrunk A. R., Megeath S. T., Wilson T. L., 1998, A&A 336, 991
Tieftrunk A. R., Wilson T. L., Steppe H., et al., 1995, A&A 303, 901
Turner J. L., Welch W. J., 1984, ApJ 287, L81
Werner M. W., Becklin E. E., Gatley I., et al., 1980, ApJ 242, 601
Wilner D. J., Welch W. J., Forster J. R., 1995, ApJ 449, L73
Wilson T. L., Gaume R. A., Johnston K. J., 1993, ApJ 402, 230
Wilson T. L., Gaume R. A., Johnston K. J., Tieftrunk A., 1995, ApJ 452, 693
Wright M. C. H., Dickel H. R., Ho P. T. P., 1984, ApJ 281, L71
Wynn-Williams C. G., 1971, MNRAS 151, 397
Wynn-Williams C. G., Werner M. W., Wilson W. J., 1974, ApJ 187, 41